JOURNAL OF MATERIALS SCIENCE 29 (1994) 356–365

Filamentary preforms of Al–13 wt % Si alloy reinforced with TiC-coated and pre-treated carbon fibres

M. DE SANCTIS, S. PELLETIER, Y. BIENVENU
Ecole Nationale Supérieure des Mines de Paris, Centre des Materiaux P. M. Fourt, RN 7-91000 Evry, France

H. VINCENT
Laboratoire de Physicochimie-Minérale I, Université Claude Bernard, Lyon-I, Villeurbanne, France

Filamentary preforms of aluminium–13 wt % Si alloy reinforced with TiC-coated carbon fibres were obtained by liquid metal infiltration using K_2ZrF_6 as wetting agent. The interfacial structure was investigated using analytical electron microscopy (TEM, SEM) and the fibre strength measured following each step of processing. The reaction between the K_2ZrF_6 deposit and the molten alloy is discussed on the basis of the reaction products formed at the fibre–matrix interface, which mainly consisted of fluoride compounds (K_3AlF_6), different zirconium-rich silicides (Si_2Zr, SiZr (Al), (Al, Si)$_2$Zr) and crystalline γ-alumina. Large amounts and/or inhomogeneous distributions of the K_2ZrF_6 deposit should be avoided, because the massive precipitation of colonies of intermetallics around fibres is conducive for the formation of harmful aluminium carbides and favours brittle fracture of the composite. The utilization of TiC-coatings formed by the reactive chemical vapour deposition process gave satisfactory results, both in terms of composite elaboration and fibre protection during liquid infiltration.

1. Introduction

Long-fibre aluminium-matrix composites (MMCs) are attractive for the aerospace industry owing to their high specific strengths, low thermal expansion coefficients and useful engineering properties at elevated temperatures. At present, the production of flexible and continuous Al–C wires or ribbons is being considered with the aim of fabricating, by hot pressing, plates/tubes in composite material with an interesting performance-to-cost ratio. Carbon fibres are the most economic of the continuous ceramic fibres, although the lack of wettability of carbon by aluminium at temperatures below 850 °C [1] and strong interfacial chemical reactions during liquid infiltration, must be properly envisaged [2, 3].

In order to enhance wetting at relatively low temperatures, one can alter either the fibre surface or the matrix with something that will promote interfacial chemical reactions and/or disrupt the oxide layer on the metal surface. Coatings that react with the matrix are numerous and, according to the particular reinforcement used, they include metallic coatings (copper, silver, nickel) [4] or ceramics (Ti–B) [5]. Moreover, there are coatings which are active mainly because they can affect the oxide covering aluminium, such as alloying additions of lithium, calcium and magnesium [6] or pre-treatments with alkali metals (Na–K/Sn–Mg) [7]. Coatings that react with the oxide layer on the metal include a deposit of K_2ZrF_6, which has been successfully used to infiltrate by simple gravity casting, SiC-based ceramic preforms at about 800 °C [8]. Patankar *et al.* [9] fabricated carbon-fibre-reinforced Al–12 wt % Si alloy composites using K_2ZrF_6, but strong fibre damage occurred during liquid-metal infiltration (LMI) and the resulting tensile properties for the bulk composite were far from those predicted by the rule of mixtures (ROM).

In this work, K_2ZrF_6 deposits were used to infiltrate with a molten Al–13 wt % Si alloy, uncoated and carbide-coated (TiC, B_4C) carbon fibres. The variation of physical–mechanical properties of fibres and the microstructure of regions at the C/Al interface have been evaluated, because both properties can strongly influence the quality of the composite material.

2. Experimental procedure

The filamentary preforms were constituted of a low-melting Al–13 wt % Si alloy (AS13) reinforced with Toray-Soficar 6K-tows of T300 carbon fibres of about 7 μm diameter. At the surface of fibres, an adherent carbide layer (TiC or B_4C) was formed using the reactive chemical vapour deposition (RCVD) process [10], where the solid carbon reacts in a continuous process at high temperatures (> 1000 °C) with a gaseous mixture of hydrogen and metallic chlorides

0022–2461

TABLE I Tensile strengths of uncoated and TiC-coated carbon fibres before and following liquid metal infiltration (gauge length 2 cm, crosshead speed 5 mm min^{-1}) (CDM Laboratory).

Fibres	σ_r (MPa)	E(GPa)	m(Weibull)
C_{T300}	2675	210	6.5
C_{T300} + 0.6 mg cm^{-2} K_2ZrF_6 + AS13	1050	210	3.8
C(TiC)	1810	210	4.7
C(TiC) + 0.2 mg cm^{-2} K_2ZrF_6 + AS13	1472	210	2.8

according to

$$M-Cl_x(g)+x/2\ H_2(g)+C_{(fib)} \rightarrow MC(s)+xHCl(g) \quad (1)$$

where, in the present work, M = Ti, B.

The pre-treatment with the wetting agent consisted of dipping bundles in K_2ZrF_6-saturated and boiling aqueous solutions, followed by drying at 100 °C for 1 h. The fibre tows were then placed inside an alumina tube, 3 mm diameter, and preheated at 600 °C under an argon atmosphere. The tube was partially plunged in the metal bath at 690 °C and the flow of liquid metal into the preform was aided by applying vacuum at the other end of the tube. The contact time between the liquid metal and the reinforcement was about 2 min.

The carbon fibres were then extracted from the composites by dissolving the alloy matrix using sodium hydroxide solutions. The fibre strength was measured by testing single fibres with a gauge length of 2 cm, glued to transparent tabs. A statistical treatment of a series of 40–60 rupture tests was carried out by the Weibull method, see Table I.

Fracture surfaces of the composite were examined using a Philips 501 scanning electron microscope (SEM) equipped with a Tracor energy dispersive X-ray spectrometer (E.O.S.). A Cameca SX50 microprobe analyser (EPMA) was also used to obtain quantitative analysis of phases on polished cross-sections of preforms (W.O.S.).

Transmission electron microscopy (TEM) studies have been carried out on samples extracted from sections parallel and transverse to the direction of the fibres. TEM specimens were prepared using standard methods and examined in a TEM–STEM Philips EM 430 instrument operating at 300 kV and equipped with a Tracor E.O.S. X-ray spectrometer.

3. Results

3.1. Preform production

Preliminary tensile tests showed that the carbide layers formed by RCVD consistently led to a decrease in the fibre strength, with a loss of 33% of the initial value for TiC-coated (C(TiC)) fibres and of about 16% for C(B_4C) fibres, see Table II. Among the fibres considered here, the C(TiC) fibres exhibited the most irregular surface with a high density of microdefects, see Fig. 1a–c.

TABLE II T300 and RCVD-coated T300 fibre strength characteristics (gauge length 2 cm, crosshead speed 0.1 mm min^{-1}) (LPCM Laboratory).

Fibres	σ_r (MPa)	E(GPa)	m(Weibull)
C_{T300}	3150	210	6.9
C(TiC)	2100	208	5.5
C(B_4C)	2650	210	4.7

All attempts to obtain LMI of fibre bundles at temperatures of 690 °C without using K_2ZrF_6 as wetting agent, were unsuccessful. On the other hand, satisfactory results have been obtained for C(TiC) fibres in terms of (i) control over the crystallization of K_2ZrF_6 onto the surface of fibres, which led to a homogeneous distribution of small-sized K_2ZrF_6 crystals (see Fig. 1b), and (ii) successful LMI of the bundles using deposits as low as 0.2 mg cm^{-2}. By comparison, uncoated and C(B_4C) fibres exhibited an uneven precipitation of large K_2ZrF_6 crystals (Fig. 1d), and C(B_4C) fibres were not infiltrated even using massive K_2ZrF_6 pre-treatments of 3 mg cm^{-2}.

Fig. 2a shows a typical transverse section of a C(TiC)-fibre reinforced Al–13 wt % Si filamentary preform. The infiltration of aluminium in the tows is satisfactory and the composite preform exhibits a low porosity level. Large silicon needles are formed in regions relatively far from fibres, whereas in regions of dense fibre packing (volume fraction $V_f \approx 40\%$), silicon particles of smaller dimension often form inter-fibre bridges (see Fig. 2b). The X-ray EPMA elemental maps in Fig. 3 show the distribution of elements on the cross-section of the preform, and the presence of some reaction products around fibres can be inferred. Zirconium is possibly combined with silicon to form intermetallics, and fluorine and oxygen are localized in the matrix close to fibres. Potassium is also present in such places and some of it appears to have diffused into the fibres: EPMA analysis of fibre interiors gave potassium contents ranging up to 3.4 wt %.

Following dissolution of the matrix, the uncoated carbon-fibres appeared heavily damaged by the formation of deep surface roots (see Fig. 4a). Tensile tests indicated, for these fibres, a loss in strength of about 61% with respect to the initial value, also in correspondence with decreased m-values, see Table I. On the contrary, C(TiC) fibres were, in most regions, still covered by the protective layer (see Fig. 4b) and the loss in strength of fibres was only 19% of the value before liquid infiltration.

Fig. 5 shows a typical fracture surface of filamentary preforms. In regions of dense fibre packing, the fracture is essentially coplanar and there is little evidence of fibre pull-out. Fibres appear to be well bonded with the surrounding matrix which, in most cases, exhibits a smooth appearance.

3.2. Analytical transmission electron microscopy

From the TEM analysis, the fibre surfaces appeared as regions of strong solute segregation, and elemental silicon and iron-rich intermetallics (mainly α-AlFeSi)

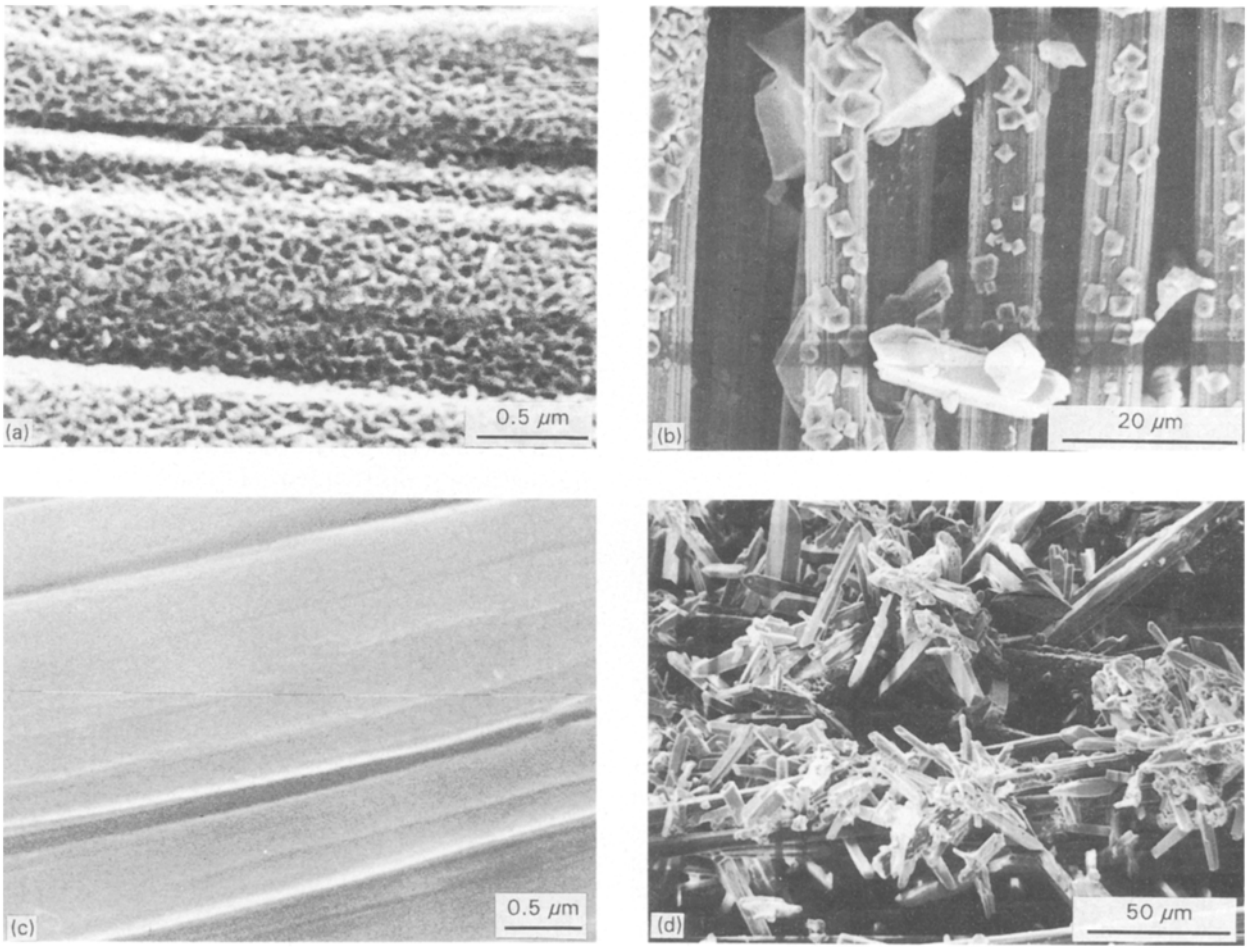

Figure 1 Scanning electron micrographs showing the surface appearance and the distribution of the K_2ZrF_6 deposit for (a, b) C(TiC) fibres, and (c, d) C(B_4C) fibres.

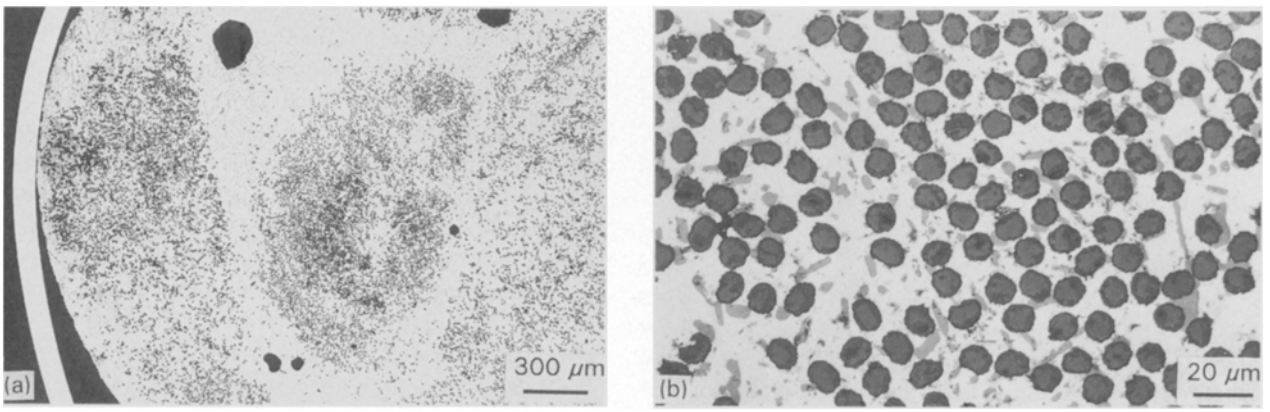

Figure 2 Optical micrographs from a transverse section of C(TiC)/AS13 preforms showing (a) satisfactory infiltration of the fibre bundles, and (b) a region of dense fibre packing ($V_f \approx 40\%$).

frequently formed at the fibre/matrix interface. This circumstance could be related to solute rejection ahead of the advancing solid–liquid interface and, therefore, the solidification front was likely to move from interfibre regions towards fibre surfaces.

The products of the reaction between K_2ZrF_6 and the molten alloy were mainly constituted of zirconium-rich silicides and fluoride compounds (detailed below) and they were always in close contact with fibres. A striking observation was an increased fibre–matrix reaction corresponding to large colonies of silicides. For uncoated fibres, such a feature was evident from the extension of the reaction zone and from the increased dimensions of interfacial lath-like aluminium carbides (see Fig. 6). For TiC-coated fibres, the localization of K_2ZrF_6 crystals favoured the disruption of the protective layer and frequently led to fibre damage. Fig. 7 is a TEM bright-field image from

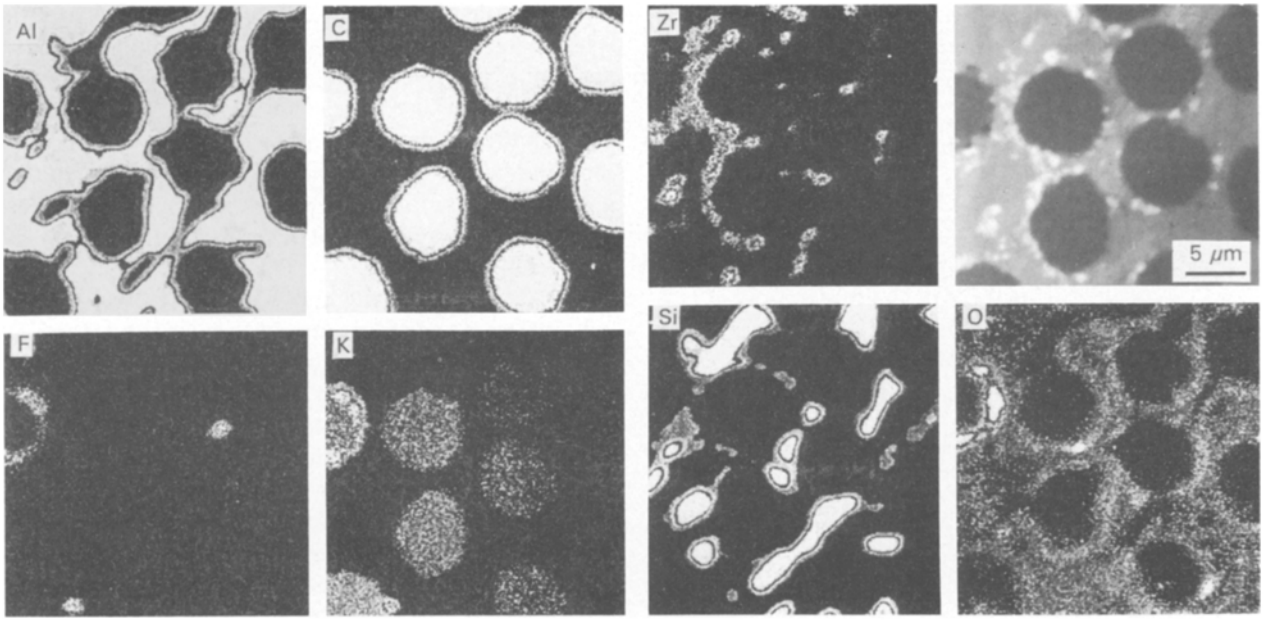

Figure 3 X-ray elemental maps from a polished section of C(TiC)/AS13 filamentary preforms.

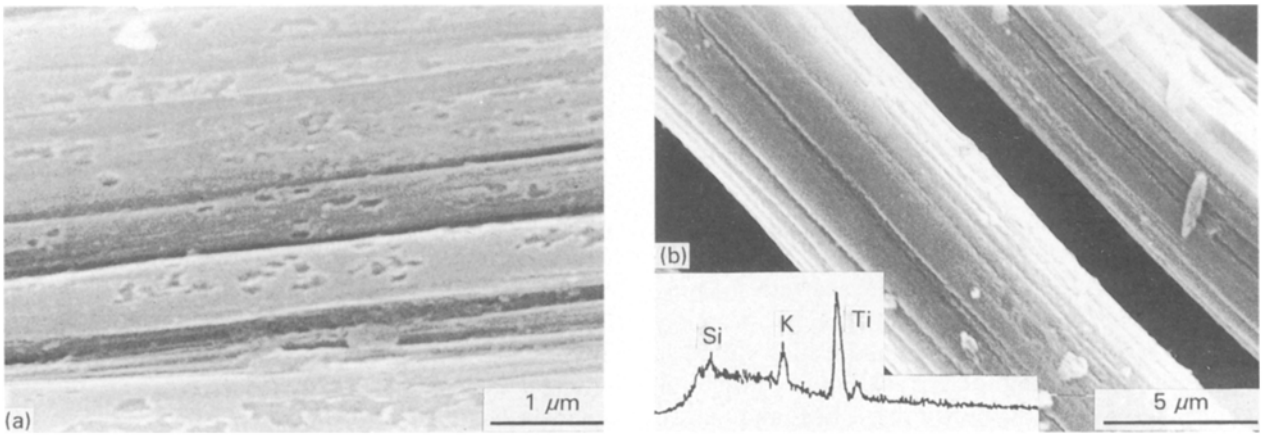

Figure 4 Scanning electron micrographs of fibres extracted from the composite: (a) uncoated and (b) TiC-coated fibres.

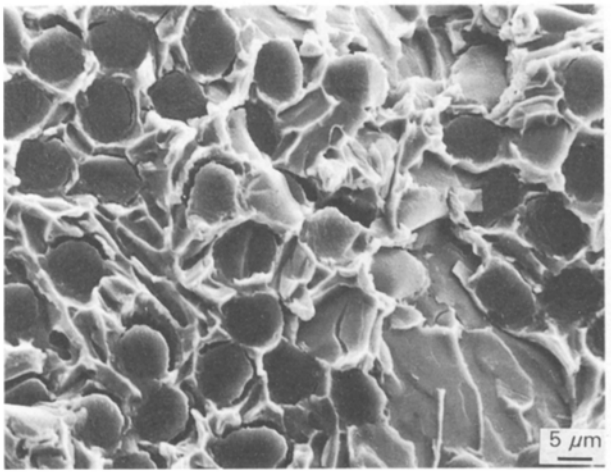

Figure 5 SEM image showing the fracture surface of filamentary preforms in regions of dense fibre packing.

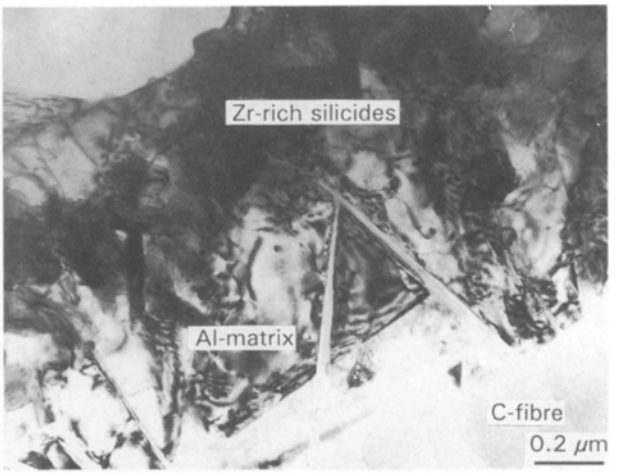

Figure 6 Transmission electron micrograph from C/AS13 interface regions (section longitudinal to fibres).

a transverse section of the preform, showing a large and twinned silicon particle between two closely spaced fibres. No significant chemical reaction took place between the silicon particle and the C(TiC) fibre, and the contact region at the fibre–matrix interface ("A" in the figure) is regular in shape. On the contrary, in regions labelled "B", where some silicide particles are visible close to the fibre, the fibre–matrix interface is

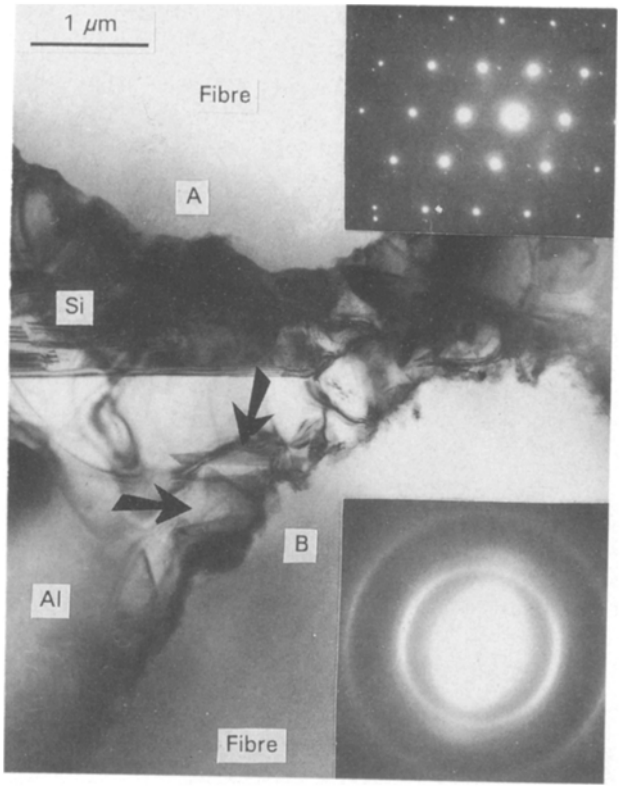

Figure 7 Transmission electron micrograph from C(TiC)/AS13 interface regions (section transverse to fibres). The SAD pattern from the twinned silicon particle is shown in the panel.

very irregular and some reaction occurred between the carbon fibre and the matrix.

Fig. 8a shows the C(TiC)/Al interface with the presence of some products resulting from the reaction between K_2ZrF_6 and the aluminium alloy. In such regions, the following phases and microstructural features have been identified by TEM and X-ray microanalyses:

1. Si_2Zr: orthorhombic with $a = 0.372$ nm, $b = 1.468$ nm, $c = 0.368$ nm, space group $Cmcm$ [11]; compositions close to 0.59Si 0.32(Zr + Ti) 0.09Al. Fig. 9a shows the selected-area diffraction (SAD) pattern with B close to the [1 0 1] zone axis from the precipitate. Si_2Zr-particles were often faulted and SAD patterns exhibited rows of reciprocal points smeared into continuous intensity lines parallel to the 0 2 0 row. These particles, as did most of the silicides reported below, contained several atomic percent of dissolved titanium;

2. $(Al, Si)_2Zr$: tetragonal with $a = 0.390$ nm and $c = 0.901$ nm, space group $I4/mmm$ [12]; chemical composition close to 0.45Al 0.35(Zr + Ti) 0.2Si. Fig. 9b shows the indexed [1 1 0] zone axis from this phase. These particles were identified only in regions where large colonies of silicides formed and they were preferentially localized away from the fibre surfaces (see Fig. 8b). The structure and composition of this phase and that of binary Si_2Zr are not as different as first appears, and it is possible that the ternary phase is basically Si_2Zr, in which the replacement of silicon by aluminium produced a small change in structure and this accounts for the different lattices reported;

3. ZrSi(Al): orthorhombic with $a = 0.378$ nm, $b = 0.991$ nm, $c = 0.375$ nm [11]; equivalent atomic percentages of (Zr + Ti) and silicon and with aluminium ranging up to 5 at %. The monosilicide ZrSi(Al) phase has been frequently observed and Fig. 9c shows the relevant [1 1 0] zone axis from this phase;

4. Al_4C_3: rhombohedral with $a = 0.333$ nm and $c = 2.499$ nm in hexagonal cell coordinates, space group $R\bar{3}m$ [11]. The aluminium carbides observed on uncoated fibres were thin laths of width less than 50 nm and length up to 1 μm. The carbides were frequently observed to penetrate towards the fibre interiors, thus being responsible for the surface roots visible in Fig. 4a. The SAD pattern reported in Fig. 9d is indexed as the [1 $\bar{2}$ 1 0] zone axis from the carbide phase and one can note the most intense reflection (0 0.1 2), corresponding to the number of basal layers in the unit cell [13]. Fig. 10 shows the lattice image of

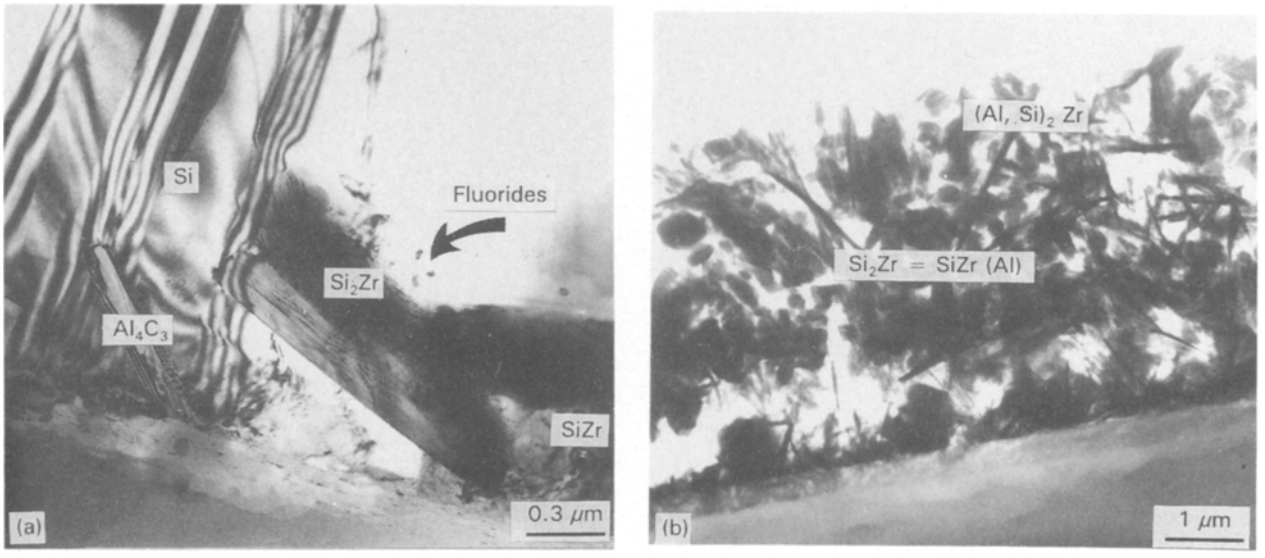

Figure 8 Transmission electron micrograph showing (a) precipitation of intermetallics at the C(TiC)/AS13 interface, (b) formation of colonies of silicides (fibre extracted from the composite).

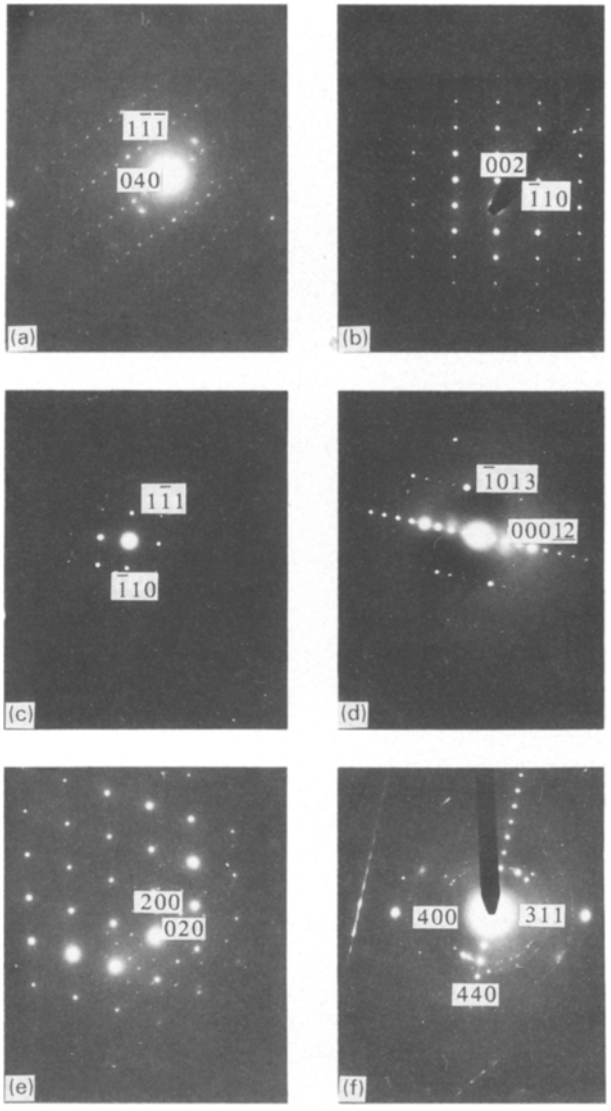

Figure 9 Indexing of SAD patterns from precipitates formed at or close to the fibre surface: (a) [1 0 1] Si_2Zr, (b) [1 1 0] (Al, Si)$_2$Zr, (c) [1 1 0] SiZr (Al), (d) [1 $\bar{2}$ 1 0] Al_4C_3, (e) [0 0 1] K_3AlF_6 (particles arrowed in Fig. 8a) (f) ring pattern from randomly oriented γ-Al_2O_3 crystallites.

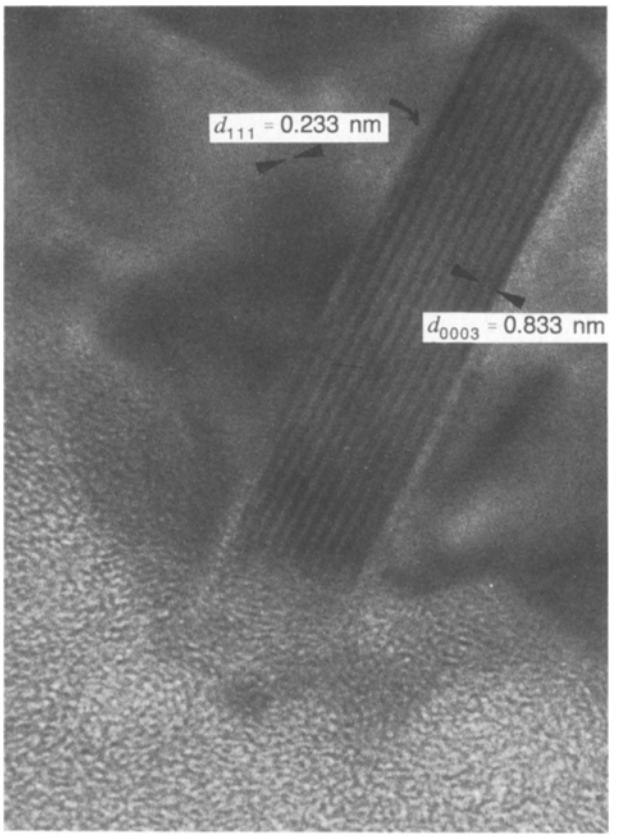

Figure 10 Lattice image of aluminium and carbide showing [1 1 1] Al and (0 0 0 3) Al_4C_3 planes.

Figure 11 Transmission electron micrograph showing strong image contrast from the matrix close to silicide particles.

both carbide and aluminium; the planes (0 0 0 3) Al_4C_3 are parallel to the longitudinal axis of the carbide. Moreover, the presence of steps along the edges of the crystal support the occurrence of a ledge mechanism of growth [14]. The existence of an orientation relationship between the carbide phase and the aluminium matrix, with (0 0 0 1) Al_4C_3 parallel to (1 1 1) Al planes, has been previously reported [14, 15]. Nevertheless, Fig. 10 clearly indicates the absence of such a systematic relationship. In the present case, the solidification front moved from the interfibre regions towards the fibres and the nucleation of solid aluminium was unlikely to occur on the surface of carbides with a preferred orientation. Finally, some evidence suggested that the nucleation of carbides took place at the fibre surface and required, for TiC-coated fibres, the local breakdown of the interlayer. For example, Fig. 14 shows a region of the fibre partially protected by the TiC-coating (see later in discussion) and the small carbide locally observed was still nucleated at the surface of the carbon fibre.

5. Fluoride compounds: EPMA analyses indicated the presence of K/F/O in regions close to the C/Al interface, see Fig. 3. A specific TEM study was possible on small particles such as arrowed in Fig. 8a,

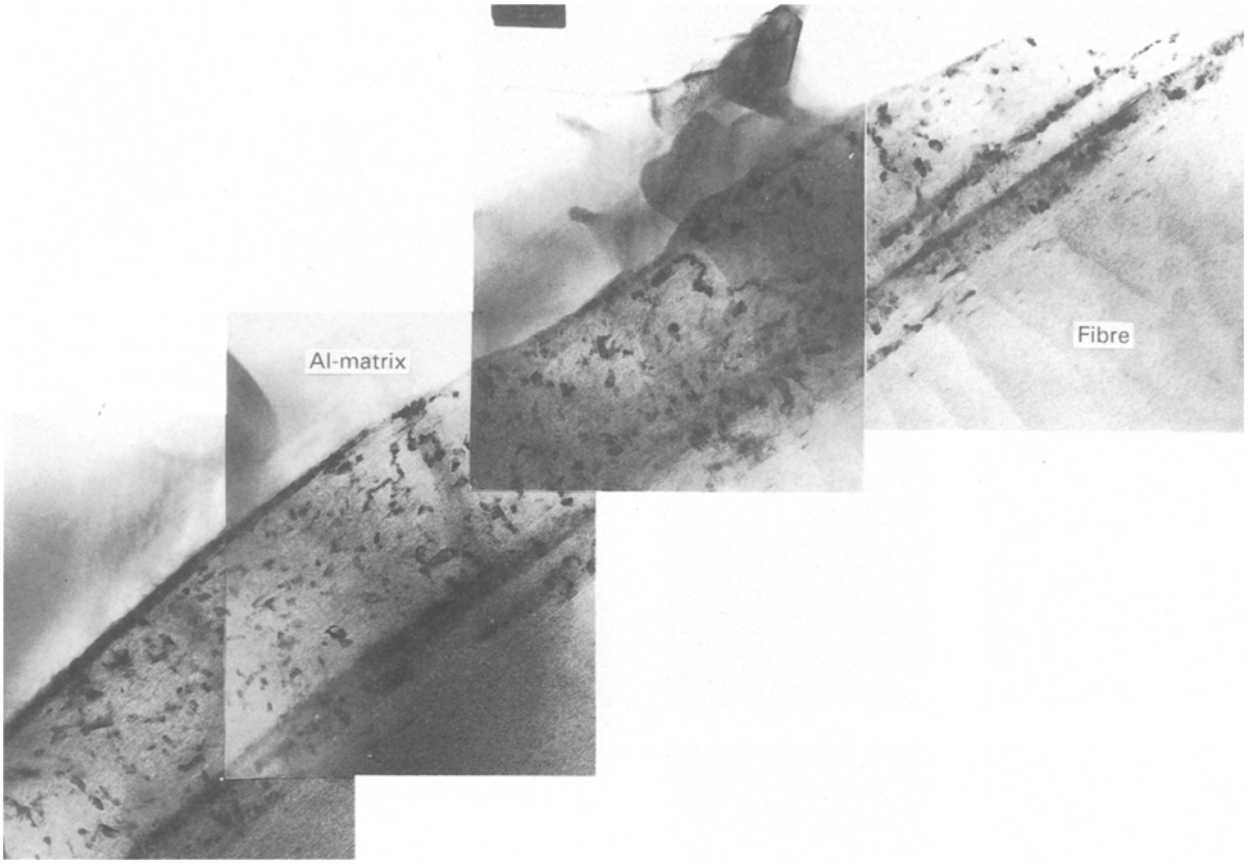

Figure 12 Montage of electron micrographs showing a fibre–matrix region with a low density of interface precipitation.

which exhibited (EDS) high potassium contents. Fig. 9e shows the SAD pattern from a prominent pole of these particles (with B also not far from [1 1 0] Al): the diffraction maxima can be indexed as the [0 0 1] zone axis from the K_3AlF_6 phase, cubic in structure with lattice parameter $a = 0.849$ nm [12];

6. Local features: the aluminium alloy matrix adjacent to colonies of silicides frequently exhibited a strong image contrast when viewed under dynamical image conditions. The most important local features observed were: (i) the presence of misfitting precipitates (Fig. 11), which reversed their white/black lobe contrast under opposite operating $\boldsymbol{g}$-vectors. At the point marked "X", EDS analysis mainly indicated high potassium contents for the matrix and, therefore, the small precipitates possibly consisted of potassium-rich fluoride compounds; (ii) the presence of cavities/gas bubbles, which exhibited the characteristic through-focus properties (bright/dark dots in under/over focused conditions); (iii) the ring diffraction pattern in Fig. 9f, which has been indexed as arising from crystalline γ-alumina. This pattern cannot have derived from superficial oxides, because these would be present in the amorphous form.

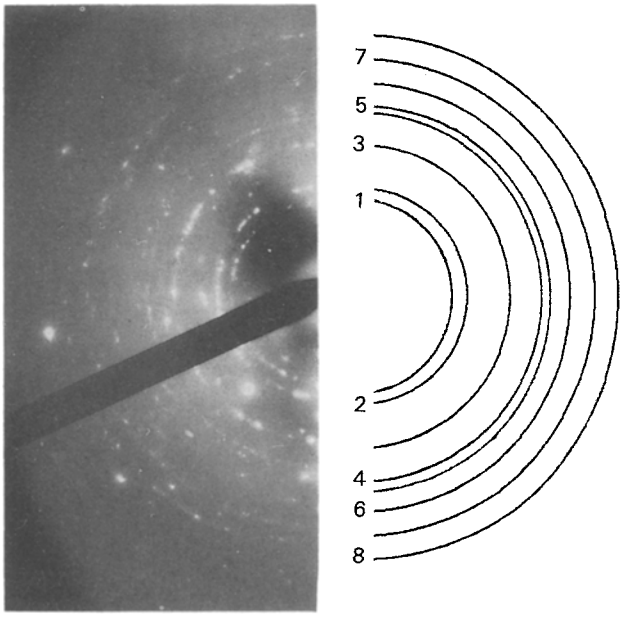

Figure 13 SAD ring pattern arising from the interfacial regions in Fig. 12. The labelling of rings is shown in Table III.

TABLE III

Ring	TiC *d*-spacings (nm)	Measured *d*-spacings (nm)
1	(1 1 1) 0.250	0.247
2	(0 0 2) 0.216	0.213
3	(0 2 2) 0.153	0.153
4	(1 1 3) 0.130	0.131
5	(2 2 2) 0.125	0.124
6	(0 0 4) 0.108	0.106
7	(0 2 4) 0.096	0.095
8	(2 4 4) 0.088	0.087

The fibre/matrix interface was quite different in regions where few, if any, zirconium-rich silicides were formed. The formation of interfacial carbides on uncoated fibres was locally reduced and it was practically absent on C(TiC) fibres. For the latter, Fig. 12 shows a montage of electron micrographs taken from a representative region. The carbide layer does not appear heavily damaged and is about 40 nm thick. The TiC coating is constituted by randomly oriented crystallites, the strongly diffracting ones appearing dark in Fig. 12. The typical SAD pattern arising from these interfacial regions is shown in Fig. 13 and the

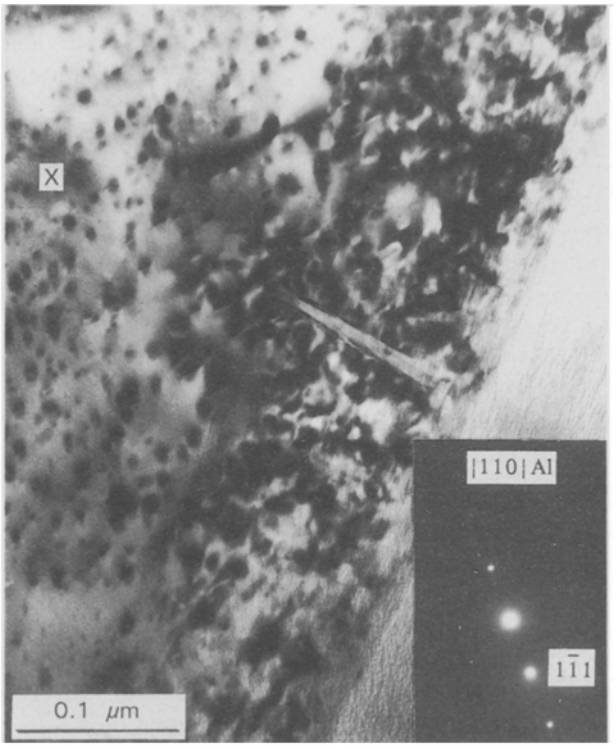

Figure 14 Transmission electron micrograph showing the occurrence of interfacial chemical reactions at the C(TiC)/AS13 interface.

indexing of rings indicates that the visible reflections correspond to all those expected for the TiC cubic phase with $a = 0.432$ nm, space group $Fm3m$ [12]. In these regions, one may infer a good adhesion between the matrix and the fibre, which was realized through the wetting of the TiC layer by the liquid metal. Fig. 14 is a high-magnification image taken under dynamic imaging conditions and the presence of misfitting precipitates with the line-of-no-contrast perpendicular to the operating g-vector is evinced. X-ray microanalysis from the region marked "X" showed titanium contents as high as 4 wt % for the matrix, which far exceeds the amount possible in aluminium solution.

4. Discussion

4.1. K_2ZrF_6 pre-treatment: origin of the wetting enhancement

From the work of Rocher *et al.* [16] and Shamm *et al.* [17], the reaction mechanism between K_2ZrF_6 and aluminium alloys can be described as follows ($T_{ref.} = 700\,^{\circ}C$)

$$3K_2ZrF_6 + 2Al_2O_3 = \text{"}6KF, 4AlF_3\text{"} + 3ZrO_2$$
$$\Delta G^{\circ} = -282.6\ \text{kJ mol}^{-1} \quad (2)$$

$$3ZrO_2 + 4Al = 2Al_2O_3 + Zr$$
$$\Delta G^{\circ} = -1.8\ \text{kJ mol}^{-1} \quad (3)$$

$$3K_2ZrF_6 + 4Al = \text{"}6KF, 4AlF_3\text{"} + 3Zr$$
$$\Delta H^{\circ} = -306.4\ \text{kJ mol}^{-1} \quad (4)$$

$$3Zr + 9Al = 3Al_3Zr$$
$$\Delta H^{\circ} = -487.2\ \text{kJ mol}^{-1} \quad (5)$$

The K_2ZrF_6 crystals and the alumina pellicula on the molten alloy should be the first species to come into contact during LMI. Reactions 2 and 3 are thermodynamically favoured and they summarize the interaction between fluoride species coming from the thermal decomposition of K_2ZrF_6 and the oxide present on the liquid metal [17]. Once the liquid metal has "wetted" the deposit, Reactions 4 and 5 proceed and complete the dissolution of the oxide layer through the formation of a cryolithic "$6KF, 4AlF_3$" Al_2O_3 mixture, immiscible with liquid aluminium. From the present work, the identification of both γ-alumina and K_3AlF_6 particles supports the formation of such a cryolithic mixture, because the decomposition of "$6KF, 4AlF_3$" in a $K_3AlF_6 + 3KAlF_4$ mixture [18] and the formation of γ-alumina crystallites is expected after cooling at room temperature.

Other factors have been indicated as important to enhance wetting [16], the most effective being a local increase in temperature due to the exothermic Reactions 4 and 5. In fact, an enhanced reaction between uncoated fibres and the matrix was always observed in regions of significant precipitation of silicides, see Fig. 6. For TiC-coated fibres, the local rise in temperature was possibly so large as to promote the dissolution of the protective layer and, subsequently, the nucleation of interfacial carbides, see Fig. 8a.

The utilization of an Al–Si alloy does not change qualitatively the reaction mechanism and just leads to the formation of zirconium-rich silicides. Rocher *et al.* [16] and Patankar *et al.* [9] claimed the formation of the Si_2Zr phase, but present findings indicate that additional phases can form, the most common being a monosilicide SiZr(Al) phase.

During LMI of fibres, a strong diffusion of potassium took place towards the interior of the fibres and the interposition of a TiC layer was rather ineffective in minimizing this effect, see Fig. 3. Potassium was still found within fibres following the dissolution of the metallic matrix, and the formation of intercalation compounds is highly probable. However, this occurrence is not expected strongly to affect the tensile strength of carbon fibres [19].

4.2. Protective TiC coating

As stated in Section 3.1, the carbide layers formed at the fibre surface by the RCVD process led to a decrease in the fibre tensile strength and this effect was particularly strong for C(TiC) fibres (see Table II). The

loss in strength would occur through carbide layer fractures at strain levels below the fracture strain of the fibre and many variables, such as the layer material, its thickness and the deposition technology are known to be important [20]. In the present work, chemical reactions occurring at the fibre surface during the RCVD process did not damage the fibres, because the loss in strength measured for C(TiC) fibres has been almost entirely recovered following oxidation in air (450 °C) of the coating [21]. On the contrary, the large number of defects of the TiC layer (Fig. 1a), and the development of surface residual stresses during cooling from the high temperatures of the RCVD process (> 1000 °C) could both favour premature failure of the coating. To reduce these effects, the interposition of pyrolitic carbon between the carbon fibre and the ceramic layer can be effective [22] and possibly considered in subsequent work.

In spite of the prolonged contact time with the molten alloy (about 2 min), the TiC layer was useful in reducing the degradation of physical–mechanical properties of fibres (see Fig. 4b). The TiC coating was unstable during liquid infiltration with molten AS13, but the fibre protection was insufficient only in regions covered by a massive deposit of K_2ZrF_6 where significant amounts of titanium were found dissolved in the zirconium-rich silicides. By comparison, the chemical reaction between the TiC layer and the molten alloy in silicide-free regions (Fig. 14), did not induce any fibre damage and it enhanced the local adhesion of the matrix to the fibre [22].

4.3. K_2ZrF_6 pre-treatment: advantages and limitations

The K_2ZrF_6 pre-treatment did not affect the fibre strength and it was strictly necessary to obtain some wetting of uncoated and C(TiC) fibres at temperatures as low as 690 °C. However, the interposition of protective coatings is strictly required, because the exothermicity of the reactions between K_2ZrF_6 and the aluminium matrix also promotes reactions at the fibre–matrix interface and favours the formation of harmful aluminium carbides, see Fig. 6.

The satisfactory results obtained with pre-treated C(TiC) fibres ($K_2ZrF_6 \approx 0.2\ mg\,cm^{-2}$) confirms that low quantities of K_2ZrF_6 would be necessary to dissolve the oxide layer on the liquid metal [17]. On the other hand, increasing fibre pre-treatments have been used to infiltrate uncoated carbon fibres ($0.6\ mg\,cm^{-2}$) and C(B_4C) fibres were not infiltrated even using massive K_2ZrF_6 deposits ($3\ mg\,cm^{-2}$). From these results, some importance should be also attached to the distribution of the K_2ZrF_6 deposit along the fibres as well to the occurrence of interfacial reactions during liquid infiltration. The control over the crystallization of K_2ZrF_6 from saturated aqueous solutions was, to some extent, feasible with C(TiC) fibres, for which the large number of surface defects acted as sites for the heterogeneous nucleation of K_2ZrF_6 crystals, see Fig. 1a. Furthermore, the chemical nature of the TiC/B_4C coatings has to be considered. ESCA analyses on RCVD carbide layers [21] showed that the composition of carbides so formed is not stoichiometric, and that titanium oxides/boron nitrides are also respectively present within TiC/B_4C layers. As the carbon content of the nearly covalent TiC_x decreases, the latter becomes more and more metallic in character and the wetting of the layer by liquid metals is favoured [23]. By comparison, the fully covalent B_4C/BN compounds are chemically more stable and they are not easily wetted by liquid metals at temperatures here considered [24]. These differentiations are important, inasmuch as the utilization of large amounts of K_2ZrF_6 would be detrimental for resulting mechanical properties of the composite material. In regions of dense fibre packing, the formation of colonies of hard and brittle intermetallics around fibres can reduce the ductility of the already brittle Al–Si matrix and also interfere with the transfer load mechanism to the fibre. Moreover, large amounts and/or inhomogeneous distributions of the K_2ZrF_6 deposit will lead to significant amounts of harmful aluminium carbides which, in turn, strongly increase the fibre–matrix bond. In fact, the fracture of composite preforms obtained here was usually planar, with little evidence of both ductility and energy dissipation mechanisms such as fibre pull-out (see Fig. 5). A better distribution of the fibre pre-treatment on C(TiC) fibres and the utilization of pure aluminium are actually considered with the aim to alleviate these problems and to optimize mechanical properties of the composite.

5. Conclusions

A pre-treatment of carbon fibres with K_2ZrF_6 allows the liquid metal infiltration of uncoated and TiC-coated carbon fibres with an Al–13 wt% Si alloy at temperatures as low as 690 °C. The fibre wettability is enhanced through the dissolution of the alumina layer on the liquid surface by fluoride compounds, which are formed together with zirconium-rich silicides (mainly Si_2Zr and SiZr(Al)). However, these reactions are exothermic and favour the degradation of physical–mechanical properties of fibres during liquid infiltration. The control over the amount and distribution of the fibre pretreatment is important in order to minimize the local fragilization of these fibres by interfacial Al_4C_3 carbides, as well the massive formation of intermetallics, which reduce local ductility of the matrix and favour brittle fracture of the composite.

Satisfactory results, both in terms of composite elaboration and fibre protection, are obtained with crystalline TiC coatings formed by the reactive CVD process. For TiC-coated fibres, only slight pre-treatments were necessary ($0.2\ mg\,cm^{-2}$), because the surface irregularities of the TiC layer favoured the heterogeneous nucleation of small K_2ZrF_6 crystals and the occurrence of chemical reactions at the TiC/AS13 interface contributed to an increase in fibre wettability.

Acknowledgements

M. De Sanctis gratefully acknowledges the financial support provided by the Italian Centro Nazionale

delle Ricerche (CNR) under the form of a research grant. The authors thank DGA-DRET, the French Defence Research Organization, for its financial support.

References

1. N. EUSTATHOPOULOS, J. C. JOUD, P. DESRE and J. M. HICTER, *J. Mater. Sci.* **9** (1974) 1233.
2. G. BLANKENBURGS, *J. Austr. Inst. Metals* **14** (1969) 236.
3. M. YANG and V. D. SCOTT, *J. Mater. Sci.* **26** (1991) 1609.
4. P. BRAKE, H. SHURMANS and J. VERHOEST, "In organic Fibres and Composite Materials – A Survey of Recent Developments" (Pergamon Press, Oxford, 1984).
5. E. G. KENDALL and R. T. PEPPER, US Pat. 4082 864 (1978).
6. N. MORI, H. SORANO, A. KITAHARA, K. OGI and K. MATSUDA, *J. Jpn. Inst. Met.* **47** (1983) 1132.
7. D. M. GODDARD, *J. Mater. Sci.* **13** (1978) 1871.
8. J. P. ROCHER, J. M. QUENISSET, R. PAILLER and R. NASLAIN, Fr. Pat. 83–0365 (1983).
9. S. N. PATANKAR, V. GOPINATHAN and P. RAMAKRISHAN, *J. Mater. Sci.* **26** (1991) 4196.
10. H. VINCENT, B. BONNETOT, J. BOUIX, H. MOURICHOUX and C. VINCENT, *J de Phys. C5* **56** (1989) 249.
11. W. B. PEARSON, "A Handbook of Lattice Spacings and Structures of Metals and Alloys-2", edited by G. V. Raynor (Pergamon Press, Oxford, 1967).
12. Powder Diffraction File, No. 3.0615 and 14.0625 International Centre for Diffraction Data, Swarthmore, USA (1988).
13. G. A. JEFFREY and V. Y. WU, *Acta Crystallogr.* **20** (1966) 538.
14. M. YANG and V. D. SCOTT, *Carbon* **29** (1991) 877.
15. A. P. DIWANJI and I. W. HALL, *J. Mater. Sci.* **27** (1992) 2093.
16. J. P. ROCHER, J. M. QUENISSET and R. NASLAIN, *ibid.* **24** (1989) 2697.
17. S. SHAMM, R. FEDOU, J. P. ROCHER, J. M. QUENISSET and R. NASLAIN, *Metal. Trans.* **22A** (1991) 2133.
18. N. W. F. PHILLIPS, R. H. SINGLETON and E. A. HOLLINGSHEAD, *J. Electrochem. Soc.* **102** (1955) 648.
19. J. B. DONNET and R. C. BANSAL,"Carbon Fibres", 2nd Edn. (Marcel Dekker, New York, 1990) pp. 249–57.
20. G. LEONHARDT, E. KEISELSTEIN, H. PODLESAK, E. THAN and A. HOFMANN, *J. Mater. Sci. Eng.* **A135** (1991) 157.
21. H. VINCENT, C. VINCENT. M. P. BERTHET, H. MOURICHOUX and J. BOUIX, *J. Less-Common Metals* **175** (1991) 37.
22. A. MORTENSEN, *J. Mater. Sci. Eng.* **A135** (1991) 1.
23. N. EUSTATHOPOULOS, D. CHATAIN and L. COUDURIER, *ibid.* **A135** (1991) 83.
24. J. V. NAIDICH, *Progr. Surf. Membr. Sci.* **14** (1981) 353.

Received 22 May 1992
and accepted 29 October 1993